THE ASTROPHYSICAL JOURNAL, 492:683–695, 1998 January 10

SIMULATIONS OF GAMMA-RAY BURSTS FROM EXTERNAL SHOCKS: TIME VARIABILITY AND SPECTRAL CORRELATIONS

A. PANAITESCU AND P. MÉSZÁROS[1]
Department of Astronomy and Astrophysics, Pennsylvania State University, University Park, PA 16802
Received 1997 March 27; accepted 1997 August 22

ABSTRACT

We compute burst spectra and time structures arising from synchrotron and inverse Compton scattering by nonthermal electrons accelerated in shocks that form during the interaction between a thin ultrarelativistic fireball and a stationary external medium. We investigate the effect of varying the most important model parameters on the resulting burst spectra, and we present a set of correlations among the spectral and temporal features of the bursts. The spectral hardness, various spectral-temporal correlations, and the spectral evolution of the simulated bursts are compared to those of observed bursts for a representative set of model parameters. Multipulse structures are simulated using a variable magnetic field and anisotropic emission, and the most important spectral and temporal properties of these pulses are compared with observations.

Subject headings: gamma rays: bursts — methods: numerical — radiation mechanisms: nonthermal

1. INTRODUCTION

The observed isotropy (Meegan et al. 1992; Briggs et al. 1996), inhomogeneity (as shown by $\langle V/V_{\max}\rangle$), and deviation from a -1.5 slope power law of the $\log N - \log P$ distribution for the fainter bursts (Meegan et al. 1992; Horack & Emslie 1994) provide string support for the hypothesis that gamma-ray bursts (GRBs) are of cosmological origin. Other observations, such as spectral hardness-brightness correlations (Mitrofanov et al. 1992a; Paciesas et al. 1992), the spectral hardness-duration anticorrelation (Kouveliotou et al. 1993), and the possible time dilation and duration-brightness anticorrelation (Norris et al. 1994, 1995; cf. Mitrofanov et al. 1996), while more equivocal, are also generally compatible with this hypothesis. The large energy that the cosmological source must release suggests that relativistic effects are likely involved in GRBs. In this paper we consider bursts that arise when an ultrarelativistic cold shell (fireball) is decelerated by interaction with the interstellar medium or a preejected slow wind. As a result of the deceleration, an ultrarelativistic blast wave ("forward shock" [FS]) propagates into the external medium (EM), transferring a substantial part of the fireball kinetic energy to the shocked EM, while another shock ("reverse shock" [RS]) propagates back into the fireball. This is the generic model that is usually referred to as the "external shock model" (Mészáros & Rees 1993). If the shell is in the linear broadening regime before it is substantially decelerated by the EM (as described by Mészáros, Laguna, & Rees 1993), a situation that is expected under a wide range of conditions, then the RS is quasi-Newtonian and therefore less efficient than the blast wave in converting the shell's kinetic energy into heat. In another very likely scenario (the "internal shock model"; Rees & Mészáros 1994; Paczyński & Xu 1994), the energy conversion takes place when several ultrarelativistic shells collide with each other, before the deceleration caused by the EM becomes important. Here we focus on the first model.

In order to simulate the propagation of the two shocks and to model the fireball-EM interaction at large Lorentz factors ($\Gamma_0 \geq 100$), we have developed a one-dimensional hybrid (finite differencing and exact Riemann solver) hydrodynamic code (Wen, Panaitescu, & Laguna 1997). As the conversion of kinetic to internal energy takes place, the heat stored in the postshock gas can be released as radiation, generating a burst. In a previous paper (Panaitescu et al. 1997) we have simulated burst light curves from fireballs with moderate Lorentz factors ($\Gamma_0 \leq 200$) using a simplified prescription for the energy release. The results were single-hump bolometric light curves with a large temporal asymmetry (light-curve decay lasting substantially longer than its rise), practically insensitive to variations of the EM density. In order to carry out an appropriate comparison of this model with the rich observational database that has been accumulated by BATSE and other experiments, we need to compute the spectra of such bursts, and to study the burst spectral evolution and its correlation with the other observational properties and parameters of the model, by taking specific energy release mechanisms into consideration. The spectral hardness of the observed bursts and their time evolution are well studied, and reproducing these should represent a major goal of any GRB model. In this work we calculate the effect of the source evolution on the burst spectrum and explore the spectral-temporal correlations predicted by the model. We also explore the physical requirements necessary for this model to produce multi-humped light curves and discuss the possible limitations. Spherical symmetry, which also describes well the case of jets with an opening angle $\theta > \Gamma_0^{-1}$, is assumed for simplicity throughout the paper. The importance of a nonplanar symmetry can be assessed from the shape of the light curves and pulses presented below.

2. MODEL PARAMETERS, ASSUMPTIONS, APPROXIMATIONS, AND SCALING RELATIONS

The most important parameters that describe the dynamics of the fireball-EM interaction and the energy release mechanism are listed in Table 1, together with the most relevant equations in which they appear. The evolution of an impulsive fireball has two phases: a free expansion phase, in which the amount of swept-up EM is small, and the deceleration caused by it can be neglected, and a

[1] Also Center for Gravitational Physics and Geometry, Pennsylvania State University.

TABLE 1

SUMMARY OF THE MOST IMPORTANT PARAMETERS AND PHYSICAL QUANTITIES THAT CHARACTERIZE THE DYNAMICS OF THE FIREBALL–EXTERNAL MEDIUM INTERACTION AND THE BURST ENERGY RELEASE

Symbol	Definition
E_0	Initial fireball kinetic energy
Γ_0	Initial fireball Lorentz factor: $E_0 = \Gamma_0 Mc^2$
$t_{\rm dec}$	Hydrodynamic timescale[a]
λ_B	Magnetic field parameter: $U_B = \lambda_B U_{\rm int}$
B	Magnetic field intensity[b]
κ	Electron-to-proton energy ratio[c]
γ_m	Minimum electron Lorentz factor[d]
$\epsilon_{\rm SY/IC}$	Comoving SY/IC photon energy[e]
$E^{\rm SY/IC}$	Detector SY/IC photon energy[f]
$Y^{\rm RS/FS}$	Kompaneets parameter[g]
$t^{\rm SY}$	Synchrotron cooling timescale[h]

[a] See eq. (1).
[b] See eq. (9).
[c] See eq. (4).
[d] See eq. (5).
[e] See eqs. (6) and (7).
[f] See eqs. (10), (11), (12), and (15).
[g] See eqs. (16), (17), and (18).
[h] See eq. (20).

decelerated expansion phase, in which the fireball kinetic energy is used to heat the swept-up EM. The fireball dynamics during the first stage were calculated analytically and simulated numerically by Mészáros et al. (1993). The evolution during this stage is determined by three parameters: (1) the energy $E_0 = 10^{51} E_{0,51}$ ergs deposited in the ejected fireball; (2) the entrained baryonic mass M, parameterized through the dimensionless entropy $\Gamma_0 = E_0/Mc^2 \gg 1$; and (3) the initial size of the fireball r_0 (which may be of the order of the neutron star radius, $r_0 \gtrsim 10^6$ cm). At the beginning of the free expansion phase, the fireball is accelerated as the radiation energy E_0 contained in it is adiabatically transformed into bulk motion energy and becomes stretched out into a thin shell. The absence of a strong burst precursor with a quasi-thermal spectrum suggests that most of the initial internal fireball energy is in the form of baryonic kinetic energy when the shell becomes optically thin and photons escape from it. Therefore, the maximum Lorentz factor attained by the fireball is $\lesssim \Gamma_0$, corresponding to a kinetic energy $\lesssim E_0$.

After the fireball Lorentz factor attains its maximum value, the fireball coasts at constant Γ_0 and later reaches optical thinness. The deceleration caused by the interaction with the EM must be taken into account when the energy stored in the shocked EM is a substantial fraction of the initial kinetic energy E_0. The shocked EM internal energy is much larger than its rest-mass energy, since its random (or thermal) Lorentz factor is $\sim \Gamma_0 \gg 1$. Throughout most of this paper we assume that the EM is homogeneous, characterized by a single parameter, its number density, $n = n_0$ cm^{-3}. The deceleration timescale in the stationary frame (with respect to the Earth) of the center of explosion (the laboratory frame) is

$$t_{\rm dec} = r_{\rm dec}/c \simeq (E_0/\Gamma_0^2\, n m_p c^5)^{1/3} \simeq 8.3 \times 10^5 E_{0,51}^{1/3}\, n_0^{-1/3} \Gamma_{0,2}^{-2/3}\ {\rm s}\ , \qquad (1)$$

where $\Gamma_0 = 10^2 \Gamma_{0,2}$. Due to the relativistic motion of the source, the stationary observer receives radiation emitted in dt in a much shorter time $dT = dt/[2\Gamma^2(t)]$ (Rees 1966), where $\Gamma(t) < \Gamma_0$ is the Lorentz factor of the shocked emitting medium. The burst duration is then approximately

$$T_b \approx 10 t_{\rm dec}/2\Gamma_0^2 = 420 E_{0,51}^{1/3}\, n_0^{-1/3} \Gamma_{0,2}^{-8/3}\ {\rm s}\ , \qquad (2)$$

where a factor of 10 was included in order to account for the progressive decrease of the flow Lorentz factor of the radiating medium. Equation (2) and the observed GRB durations imply that $100 \lesssim \Gamma_0 \lesssim$ a few $\times$ 1000. It also shows that the burst peak flux F_p satisfies $F_p (\sim E_0 D^{-2} T_b^{-1}) \propto E_0^{2/3} \Gamma_0^{8/3} n^{1/3} D^{-2}$, where D is the distance to source, if most of the available energy E_0 is radiated.

The dynamics and energetics of the deceleration phase were calculated by Rees & Mészáros (1992) and Sari & Piran (1995). For computational efficiency, the numerical simulations presented here were started from $0.5 t_{\rm dec}$, when only $\simeq 12\%$ of the EM mass within $r_{\rm dec}$ had been swept up, and the deceleration prior to this time can be safely neglected. At $t = 0.5 t_{\rm dec}$, the only physical parameter that depends on r_0 is the internal pressure P of the fireball, and, in fact, this pressure is irrelevant, as long as the shell is cold ($P \ll \rho c^2$, where ρ is rest-mass density). Therefore, the hydrodynamics of the shell-EM collision are characterized by the set of three parameters (E_0, Γ_0, n).

In the comoving frame the shocked EM has typical densities $\sim 10^3$ particles cm^{-3} and can radiate away its internal energy through synchrotron radiation (SY) and inverse Compton (IC) scattering of the SY photons in the presence of a modest magnetic field. Such mechanisms were considered by Mészáros, Rees, & Papathanassiou (1994), who studied the spectral properties of bursts arising from external shocks, and by Sari, Narayan, & Piran (1996), who derived constraints on the radiation mechanisms' parameters from the variability observed in most bursts and from efficiency considerations. The galactic magnetic field, even when compressed behind the FS, would be too weak to lead to efficient radiation. However, a frozen-in magnetic field present in the fireball (and therefore in the fluid behind the RS) would allow the post-FS material to cool by IC scattering of the SY photons coming from the post-RS medium. The swept-up EM could radiate even more efficiently if a random turbulent magnetic field built up in it. In our calculation we use this latter scenario for simplicity. Moreover, a frozen-in magnetic field will usually have only a fraction of the strength of a turbulent magnetic field at equipartition (when the magnetic field energy density is equal to the internal energy density of the gas).

We use the following assumptions and approximations in order to simulate the emission of SY and IC photons from the gas behind the two shocks:

1. The magnetic field B is parameterized relative to the internal energy density $U_{\rm int}$: $U_B = \lambda_B U_{\rm int}$, where $U_B = B^2/8\pi$ is the magnetic field energy density. For strong shocks, equation (8), derived by Blandford & McKee (1976), yields $U_{\rm int} = 3 \times 10^{-3} n_0 \Gamma_{\rm FS}^2$ ergs cm^{-3}, where $\Gamma_{\rm FS}$ is the Lorentz factor of the FS shock, so that $B = 0.27 \lambda_B^{1/2} n_0^{1/2} \Gamma_{\rm FS}$ G. Since the postshock fluids are very close to hydrostatic equilibrium, $U_{\rm int}$, and therefore B, have almost the same values behind both shocks.

2. Shock acceleration leads to a power-law distribution of electrons:

$$d\mathcal{N}_e(\gamma_e) = C \gamma_e^{-p}\, d\gamma_e\ , \quad \text{and } \gamma_m \le \gamma_e \le \gamma_M\ , \qquad (3)$$

where γ_e is the random electron Lorentz factor, and $\mathcal{N}_e$ is the number density of electrons. Such a distribution is initialized in every grid cell after it is swept up by one of the two shocks, and its subsequent evolution is determined solely by the SY and IC losses. Therefore, we do not take into account adiabatic losses or further energy exchange between protons and electrons. The former simplification is justified by the fact that the electron cooling timescale is much lower than the dynamic timescale (as shown below). We have taken $\gamma_M/\gamma_m = 10$, because the cooling timescales for larger γ_M would be too short ($\lesssim 10^{-5} t_{\rm dec}$, typically), and it would require a large computational effort to follow the evolution of these very energetic electrons accurately. The effect of a larger ratio γ_M/γ_m on the burst spectrum can be easily estimated in the figures presented in the § 3. Moreover, if Γ_0 is not low (≈ 100), or if the magnetic field is not weak or the shock acceleration inefficient (i.e., low γ_m), the most energetic electrons radiate at energies above the upper limit of the BATSE window (10 keV–a few MeV). The power-law index p was chosen to be 3.

3. The minimum electron random Lorentz factor γ_m is determined by a parameter κ that is the ratio of the energy in electrons to that of the monoenergetic protons (with Lorentz factor γ_p) after shock acceleration:

$$\int_{\gamma_m}^{\gamma_M} d\mathcal{N}_e(\gamma_e) m_e(\gamma_e - 1) = \kappa n_p m_p(\gamma_p - 1) , \tag{4}$$

where n_p is the density of protons. Using the equality of the sum of the electronic and protonic partial pressures and the total pressure (determined by the hydrodynamics of the fireball-EM interaction), γ_m and the electron distribution are completely determined:

$$\gamma_m(\kappa) = 3[(p-2)/(p-1)][(1 - X^{1-p})/(1 - X^{2-p})] \times f_\kappa (m_p/m_e)(P/\rho c^2) , \tag{5}$$

where $X = \gamma_M/\gamma_m$ and $f_\kappa = \kappa/(\kappa + 1)$. This result is valid for $\gamma_p \gg 1$ (equivalent to $P \gg \rho c^2$, which is true for the fluid behind the FS). A similar result can be obtained in the limit $\gamma_p - 1 \ll 1$ (i.e., $P \ll \rho c^2$, which is correct for the fluid behind the RS). For the ultrarelativistic FS, equations (8)–(10) of Blandford & McKee (1976) lead to $P/\rho c^2 = 0.24\Gamma_{\rm FS}$ and $\gamma_{m,\rm FS} = 660 f_\kappa \Gamma_{\rm FS}$. Mészáros et al. (1993) have shown that the evolution of the fireball thickness Δ during the free expansion phase and for $r > r_0 \Gamma_0^2 = 10^{10} r_{0,6} \Gamma_{0,2}^2$ cm is $\Delta = r/\Gamma_0^2$. This leads to a fireball density at $r \sim r_{\rm dec}$ that is much larger than that of the EM and produces a mildly relativistic RS. Numerically, we found that the Lorentz factor of the RS in the frame of the yet unshocked fluid is practically independent of Γ_0: $\Gamma_{\rm RS} \simeq 1.1$. In this case it can be shown that $P/\rho c^2 \simeq 4 \times 10^{-2}$, which leads to $\gamma_{m,\rm RS} \simeq 100 f_\kappa$.

4. In the comoving frame, the SY radiation emitted by any electron is approximated as monochromatic, with a frequency equal to the peak frequency ν_c (averaged over the pitch angle) of the SY spectrum emitted by an electron with Lorentz factor $\gamma_e(t)$ (that evolves in time, as the electron loses energy):

$$\varepsilon_{\rm SY} \simeq 4.0 \times 10^{-9} \gamma_e^2(t) B \text{ eV} . \tag{6}$$

The electron cooling and continuous electron injection will produce spectra that are flatter than the spectrum of the SY radiation emitted by a single electron below and above the peak frequency ν_c [$\nu F_\nu \propto \nu^{4/3}$ and $\nu F_\nu \propto \nu^{3/2} \exp(-\nu/\nu_c)$, respectively], so that the effect of integrating over time and over electron distribution hinders the features of a single electron spectrum. Thus, this approximation is in fact better than it first seems.

5. The spectrum of the SY photons upscattered in the Thomson regime is also approximated as monochromatic at the average energy of the IC spectrum for $\gamma_e(t)$:

$$\varepsilon_{\rm IC} = 4/3 \gamma_e^2(t) \varepsilon_{\rm SY} . \tag{7}$$

The Klein-Nishina (KN) effect on the scattering of SY photons with energies comparable to or larger than $m_e c^2/\gamma_e(t)$ is taken into account. The SY energy density $U_{\rm SY}$, necessary for calculating the IC losses, is computed as an integral over the volume of the shocked media of the SY local output. There is a strong relativistic beaming of the SY photons resulting from the radial motions of the origin of a given photon and the place where the scattering occurs: as seen from the comoving frame of the upscattering region, the SY source is moving away, unless the two regions (of SY emission and of IC scattering) are moving in the same radial direction. We assumed that the $U_{\rm SY}$ spectrum is monochromatic at the peak frequency of the SY spectrum generated by the most numerous (and least energetic) electrons that are in the same volume element in which the IC scattering takes place. This approximation is justified to some extent by the aforementioned strong relativistic beaming and the geometrical dilution of the SY output, which should make the contribution to the $U_{\rm SY}$ of the SY emission from the vicinity of IC scattering place dominant. Because of this assumption, the IC spectra shown in § 3 are calculated using only the following combinations: (i) SY-RS photons scattered on electrons accelerated by the RS and (ii) SY-FS photons scattered on electrons accelerated by the FS. The mixed combinations (iii) SY-RS photons scattered by FS electrons and (iv) SY-FS photons scattered by RS electrons are not taken into account. We will assess the effect of neglecting the last two combinations on the computed spectra.

The approximation of taking the SY and IC spectra of a single electron and that of the SY photon field to be upscattered as monochromatic is made for computational efficiency. The results presented in the § 3 were obtained from numerical runs of a few hours on a Sparc Sun 20 Station for the lowest Γ_0 considered ($\Gamma_0 = 100$), up to few days for the highest Γ_0 we used ($\Gamma_0 = 800$). Most of this computational effort is used to calculate the burst spectrum by integrating over the volume of the shocked fluid (which reduces to integrating over the radial coordinate and the angle relative to the line of sight toward the center of symmetry) and over the electron distribution in each infinitesimal volume element, and repeating this triple integral after a time short enough to treat accurately the evolution of the most energetic electrons (which have the shortest cooling timescale). Adding another integral within the triple integral, in order to include the real SY or IC spectrum from a single electron, would lead to excessively long runs.

The above analytic considerations and approximations allow us to calculate the energy E_p at the peak of the power per logarithmic energy interval (νF_ν) for the SY and IC spectra from both shocks, as seen from the detector frame. Numerically, we found that about 50% of the total energy released by a burst is emitted from $t = 1 t_{\rm dec}$ to $t = 1.5 t_{\rm dec}$. During this time, $\Gamma_{\rm FS}$ decreases from $\simeq 0.6\Gamma_0$ to $\simeq 0.4\Gamma_0$;

therefore, to a good approximation, $\Gamma_{\rm FS} \simeq \Gamma_0/2$, so that

$$\gamma_{m,\rm FS} \simeq 1.3 \times 10^5 f_\kappa (\Gamma_0/400) , \quad (8)$$

and

$$B \simeq 54 \lambda_B^{1/2} n_0^{1/2} (\Gamma_0/400) \ {\rm G} . \quad (9)$$

Taking into account that the relativistic motion of the radiating fluid boosts the comoving energy by a factor that is between Γ (if the fluid moves at an angle Γ^{-1} from the line of sight toward the fireball's center) and 2Γ (if the fluid moves on this line of sight), where $\Gamma \simeq 0.7\Gamma_{\rm FS}$ is the flow Lorentz factor of the shocked fluid, for the SY-RS radiation we obtain

$$E_p^{\rm SY,RS} \simeq 0.4 f_\kappa^2 \lambda_B^{1/2} n_0^{1/2} (\Gamma_0/400)^2 \ {\rm eV} . \quad (10)$$

The comoving energy of the SY-RS photons, $\varepsilon_{\rm SY,RS} = 2 \times 10^{-3} f_\kappa^2 \lambda_B^{1/2} n_0^{1/2} (\Gamma_0/400)$ eV, is well below the limit for KN scattering, $m_e c^2/\gamma_{m,\rm RS} = 5 f_\kappa^{-1}$ keV; therefore,

$$E_p^{\rm IC,RS} \simeq 6 f_\kappa^4 \lambda_B^{1/2} n_0^{1/2} (\Gamma_0/400)^2 \ {\rm keV} . \quad (11)$$

The SY photons emitted by post-FS electrons with Lorentz factor $\gamma_{m,\rm FS}$ arrive at the detector at

$$E_p^{\rm SY,FS} \simeq 800 f_\kappa^2 \lambda_B^{1/2} n_0^{1/2} (\Gamma_0/400)^4 \ {\rm keV} , \quad (12)$$

and, in the comoving frame, are too energetic to be upscattered in the Thomson regime: $\varepsilon_{\rm SY,FS} = 4 f_\kappa^2 \lambda_B^{1/2} n_0^{1/2} (\Gamma_0/400)^3$ keV $\gg m_e c^2/\gamma_m = 4 f_\kappa^{-1} (\Gamma_0/400)^{-1}$ eV, as long as

$$\log \Gamma_{0,2} + \tfrac{3}{4} \log f_\kappa + \tfrac{1}{8} \log \lambda_B + \tfrac{1}{8} \log n_0 \gtrsim -0.15 . \quad (13)$$

Let us assume that inequality (13) is satisfied (we argue below that it must be, for an efficient burst). The energy $m_e c^2/\gamma_e$ is a good measure of the photon energy above which the KN reduction is very effective, in the sense that it drastically reduces the intensity of the IC component. The upscattered radiation will be emitted when the FS electrons have cooled sufficiently, so that $\varepsilon_{\rm SY,FS}(\gamma_e) \le m_e c^2/\gamma_e$, implying $\gamma_e \le \gamma_{\rm KN} = 5 \times 10^4 B^{-1/3}$, where B is lower than was estimated above (eq. [9]), as the shocked material has lost some internal energy. To a good approximation, this fraction can be taken to be $\frac{1}{2}$, so that $\gamma_{\rm KN} = 1.5 \times 10^4 \lambda_B^{-1/6} n_0^{-1/6} (\Gamma_0/400)^{-1/3}$. The SY radiation emitted by FS electrons that are cold enough to scatter their own SY photons in a mild KN regime have a detector frame energy that is less than

$$E_{\rm KN}^{\rm SY,FS} \simeq 7 \lambda_B^{1/6} n_0^{1/6} (\Gamma_0/400)^{4/3} \ {\rm keV} , \quad (14)$$

which gives the peak energy of the upscattered spectrum from the FS:

$$E_p^{\rm IC,FS} \approx 0.6 \lambda_B^{-1/6} n_0^{-1/6} (\Gamma_0/400)^{2/3} \ {\rm TeV} . \quad (15)$$

The optical depth for Thompson scattering of the shocked fireball is $\tau_{\rm RS} = E_0 \sigma_{\rm Th}/4\pi m_p c^2 r_{\rm dec}^2 \ \Gamma_0 \simeq 10^{-6} E_{0,51}^{1/3} n_0^{2/3} (\Gamma_0/400)^{1/3} \ll 1$. The effect of IC scattering on the SY-RS spectrum and on electron cooling can be assessed through the Kompaneets parameter $Y^{\rm RS} = \gamma_{m,\rm RS}^2 \tau_{\rm RS}$:

$$Y^{\rm RS} \simeq 10^{-2} f_\kappa^2 E_{0,51}^{1/3} n_0^{2/3} (\Gamma_0/400)^{1/3} \ll 1 . \quad (16)$$

Calculating a similar Kompaneets parameter for the FS is more difficult, because electrons accelerated earlier can be so cold as to scatter their own SY photons in the Thomson regime, while more recently accelerated electrons are very energetic and scatter their SY photons in the extreme KN regime. A simple way of obtaining upper limits for this parameter would be to assume that all electrons have the same random Lorentz factor, and that the upscattering takes place at the limit between the Thomson and the KN regimes. [At a given energy ε_0 of the incident photon, the Kompaneets parameter for electrons colder than $\gamma_0 = m_e c^2/\varepsilon_0$ increases as γ_e^2, while for electrons with random Lorentz factors above γ_0, the same parameter increases as $\ln(2\gamma_e/\gamma_0)$.] The SY photons emitted by electrons with $\gamma_{m,\rm FS}$ (eq. [8]) are upscattered in this mild KN regime by electrons that have $\gamma_e = 140 f_\kappa^{-2} \lambda_B^{-1/2} n_0^{-1/2} (\Gamma_0/400)^{-3}$; for such scatterings the Kompaneets parameter is

$$Y^{\rm FS} \approx 10^{-5} f_\kappa^{-4} \lambda_B^{-1} E_{0,51}^{1/3} n_0^{-1/3} (\Gamma_0/400)^{-20/3} \ll 1 . \quad (17)$$

Before reaching the γ_e calculated above, electrons are cold enough to scatter the SY photons that they produce (see equation for $\gamma_{\rm KN}$ above). Assuming again that all electrons are monoenergetic and have $\gamma_e = \gamma_{\rm KN}$, the Kompaneets parameter is

$$Y_{\rm KN}^{\rm FS} \approx 10^{-1} \lambda_B^{-1/3} E_{0,51}^{1/3} n_0^{1/3} (\Gamma_0/400)^{-4/3} . \quad (18)$$

For electrons colder than $\gamma_{\rm KN}$, the Y-parameter should increase as γ_e^2, while for more energetic electrons, it should decrease as γ_e^{-4}. Thus, equation (18) gives an upper limit on the expected intensity of the IC-FS component, relative to that of the SY-FS emission. In deriving equations (17) and (18), we approximated the mass of the swept-up EM by a fraction $1/\Gamma_0$ of the fireball mass. We can conclude from equations (16) and (17) that the IC emission is not expected to alter the intensity of the SY radiation from the two shocks substantially or the synchrotron cooling timescale of electrons.

The energy release mechanisms considered in this model involve only two important parameters (κ, λ_B), which, based on equation (12), must satisfy the double inequality

$$0.1 \lesssim \log \Gamma_{0,2} + \tfrac{1}{2} \log f_\kappa + \tfrac{1}{8} \log \lambda_B + \tfrac{1}{8} \log n_0 \lesssim 0.7 , \quad (19)$$

to ensure that the burst fluence in the BATSE window corresponds to a significant fraction of the total energy radiated by the source. In the laboratory frame, the synchrotron cooling time of the least energetic FS electrons is $t^{\rm SY} = (3 m_e c/8\sigma_{\rm Th} U_B \gamma_m)\Gamma \simeq 140 f_\kappa^{-1} \lambda_B^{-1} n_0^{-1} (\Gamma_0/400)^{-2}$ s, or

$$t^{\rm SY} \simeq 4 \times 10^{-4} f_\kappa^{-1} \lambda_B^{-1} n_0^{-2/3} E_{0,51}^{-1/3} (\Gamma_0/400)^{-4/3} t_{\rm dec} . \quad (20)$$

If the SY cooling timescale is larger than the hydrodynamic timescale $t_{\rm dec}$, the progressive fluid deceleration and the adiabatic cooling of the shocked fluid lead to a softening of the spectrum (less energetic electrons and lower Doppler blueshift) and reduce the burst intensity (less energy radiated away by electrons). The end result is a weak, soft, and possibly undetectable burst. Therefore, efficiency considerations also require that $t^{\rm SY} < t_{\rm dec}$, which, using equations (1) and (20), leads to

$$\log \Gamma_{0,2} + \tfrac{3}{4} \log (f_\kappa \lambda_B) + \tfrac{1}{4} \log E_{0,51} + \tfrac{1}{2} \log n_0 > -1.9 . \quad (21)$$

Note that if this condition is satisfied by the electrons with the minimum random γ_m, then it is also satisfied by the more energetic electrons (with $\gamma_e > \gamma_m$).

The observed burst durations determine the range of Γ_0 (from eq. [2] and 10 ms $\lesssim T_b \lesssim$ 1000 s, so that $100 \lesssim \Gamma_0 < 5000$); thus, equations (19) and (21) can be used to constrain the energy release parameters (λ_B, κ). Numerical simulations for fireball Lorentz factors $\Gamma_0 > 1000$ require a large

computational effort, so hereafter we will restrict our attention to cases with $\Gamma_0 < 1000$, which give burst durations $T_b \gtrsim 1$ s (from eq. [2]), i.e., the bursts that are most often considered in the GRB statistics. For such initial Lorentz factors, κ must be larger than 10^{-2}, and λ_B should not be less than 10^{-4}, in order to give a spectral peak in the BATSE window. The burst fluence in the BATSE window is also determined by the fraction of the available energy E_0 that is radiated at a power that is large enough to give, at the detector, a photon flux above a given threshold. It would be wrong to assume that this fraction is strictly proportional to $f_\kappa = \kappa/(\kappa + 1)$, the fractional energy in electrons after shock acceleration, because even if electrons and protons are completely "decoupled" after shock acceleration (i.e., there is no further energy flow from protons to the rapidly cooling electrons), the heat stored in protons drives forward the FS, which accelerates new electrons. In this indirect way a substantial fraction of proton energy can be transferred to electrons and radiated. Numerically, we found that in $\Delta t = 2t_{\rm dec}$, a burst with $\kappa = 0.1$ and $\lambda_B = 1$ radiates $\approx 50\%$ of the total energy E_0, which is not much less than the $\approx 80\%$ of E_0 that a burst with $\kappa = 1$ and $\lambda_B = 1$ radiates during the same time. For this reason it can be considered that κ does not have an important effect on the energy released, as long as it is not much less than 10^{-1}.

It is easy to see that if most of the SY-FS radiation is in the BATSE window (i.e., eq. [19] is satisfied), then either the KN effect reduces the IC emission severely (eq. [13] is fulfilled), or the Kompaneets parameter $Y^{\rm FS}$ (eq. [17]) is less than 1. This means that if a burst observed by BATSE represents the SY radiation emitted by the shocked EM, then the IC-FS radiation from the same fluid is less energetic than the SY-FS emission, and it can be safely neglected in calculating the cooling timescale. On the other hand, if equation (13) is not satisfied (i.e., the KN cutoff does not reduce the efficiency of IC scattering behind the FS), then the SY-FS radiation does not arrive in the BATSE window. This suggests that a burst visible to BATSE can also be obtained from the IC-FS radiation, if the efficiency conditions (1) 10 keV $\lesssim E_p^{\rm IC,FS} \lesssim$ a few MeV, (2) $Y^{\rm FS} > 1$, and (3) $t_{\rm cool}^{\rm IC} < t_{\rm dec}$ are simultaneously satisfied (condition [3] is relevant for the burst efficiency only if condition [2] is satisfied). It can be easily shown that condition (1) implies upscattering in the Thomson regime, and that it cannot be fulfilled at the same time as condition (2). In other words, any combination of parameters $100 \lesssim \Gamma_0 \lesssim 5000$, $10^{-2} \lesssim \kappa \leq 1$, $\lambda_B \leq 1$, $E_{0,51} \sim 1$, and $n_0 \sim 1$ leads either to an IC-FS component that contains a substantial fraction of the available energy but is at energies larger than those visible to BATSE, or to an IC-FS radiation that arrives mainly in the BATSE window, but is much less energetic than the SY-FS radiation emitted by the burst, because of a small Kompaneets parameter. Thus the observed bursts could be IC-FS radiation only if the initial fireball kinetic energy is much larger than 10^{50} ergs sr^{-1}, in which case a much more energetic emission should be detected at energies lower than the BATSE window. Similar conclusions have been reached previously by Sari et al. (1996).

In principle, two other model parameter constraints can be obtained, if it is required that all electrons be confined in the shocked fluid, and that the duration $t_{\rm acc}$ of the electron acceleration process be much shorter than the corresponding SY cooling timescale, ensuring that electrons can reach factors γ_e larger than the post-FS γ_m derived above. The former condition requires the electron gyration radius $R_g = \gamma_e m_e c^2/eB$ to be less than the comoving shell thickness $\gtrsim r_{\rm dec}/\Gamma_0$ of the shocked fluid shell, while the latter condition requires that $t_{\rm acc} \sim \Gamma R_g/c \ll t^{\rm SY}$. It can be shown that if the inequalities (19) and (21) are satisfied, then electrons are indeed confined in the shocked fluid and are accelerated on a timescale much shorter than the SY cooling timescale, so that these two conditions do not introduce any new constraints on model parameters.

The total set of model parameters used in the simulations below is (E_0, Γ_0, n; κ, λ_B; D), including the luminosity distance to source, to which the parameter γ_M/γ_m could be added in some special cases. In the following numerical results, $D = 10^{28}$ cm; however, the cosmological redshift effect was not specifically accounted for, because the spectral redshift and temporal dilation can be included in the model independently of the hydrodynamic simulation. Therefore, the temporal-spectral correlations discussed below are not of cosmological origin; they are intrinsic properties of the bursts.

3. RESULTS AND COMPARISON WITH OBSERVATIONAL DATA

A hardness-brightness correlation, hardness-duration anticorrelation, and brightness-duration anticorrelation are straightforward predictions of these external shock models. From equations (2) and (12), and the fact that the peak flux scales as $F_p \propto E_0^{2/3}\Gamma_0^{8/3}n^{1/3}D^{-2}$, we see that the fireball's initial Lorentz factor Γ_0 ($100 \leq \Gamma_0 \lesssim$ a few $\times 10^3$) is the parameter with the strongest influence on the spectral and temporal burst properties. If the other parameters have a relatively narrow range ($1 \leq E_{0,51} \lesssim 10$, $n_0 \approx 1$) or are within the limiting values suggested above ($0.1 \leq \kappa \leq 1$, $10^{-4} \leq \lambda_B \leq 1$), then the correlations or anticorrelations expected among the burst parameters result from their Γ_0 dependence and are $E_p \propto F_p^{3/2}$, $E_p \propto T_b^{-3/2}$, and $F_p \propto T_b^{-1}$. Evidence for a hardness-brightness correlation has been presented (Mitrofanov et al. 1992a; Paciesas et al. 1992; Nemiroff et al. 1994; Pelaez et al. 1994; Mallozzi et al. 1995), as is implied by the hardness ratios, break energy, or E_p dependencies on the peak count rate or brightness class shown in these articles. A quantitative comparison is not easy, as authors seldom use F_p and E_p in their analyses (or at least the same definition of the burst hardness); nevertheless, it appears that the observed correlation is weaker than predicted above. The hardness-duration anticorrelation is observed by Dezalay et al. (1992) and Kouveliotou et al. (1993; cf. Band et al. 1993), while the evidence for a brightness-duration anticorrelation is controversial (Norris et al. 1995; Mitrofanov et al. 1996). If present, it is probably far weaker than is indicated by the above analytic scaling. Of course, a distance dispersion of an order of magnitude, as well as a broad luminosity function (variations of E_0, λ_B, and κ parameters among bursts) and evolutionary effects, would all tend to mask such an F_p-T_b anticorrelation through the parameter Γ_0.

Further comparison with observational data can be made, using numerical results. Figure 1 shows spectra (computed as flux-weighted averages of 10 instantaneous spectra, uniformly distributed within T_b) generated with different values of Γ_0 when the other parameters are held constant. The IC component from the RS is shown separately, while the other components can be distinguished in the spectrum and are identified in this figure. Note that most of

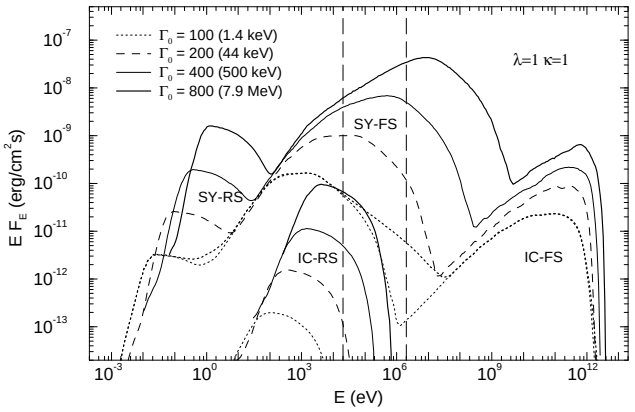

FIG. 1.—SY and IC spectra for $E_0 = 10^{51}$ ergs, $n = 1$ cm^{-3}, $D = 10^{28}$ cm, $\lambda_B = 1$, $\kappa = 1$, $\gamma_M/\gamma_m = 10$, $p = 3$, and different parameters Γ_0. The thick-dotted curve is for $\Gamma_0 = 100$ and $\gamma_M/\gamma_m = 100$. Labels indicate the origin of each component: SY = synchrotron; IC = inverse Compton scattering; RS = reverse shock; and FS = forward shock. $EF_E = \nu F_\nu$ is the power per logarithmic energy (or frequency) interval. Vertical dashed lines show the BATSE window. The legend also gives the spectral peak energy E_p for each parameter Γ_0.

the burst energy is in the SY component from the FS, and that an important fraction of this energy arrives at the detector in the BATSE window, if the parameters λ_B and κ are close to their maximum values (as predicted by eq. [19]). The ratio γ_M/γ_m is relevant for the burst fluence in the BATSE window only for $\Gamma_0 = 100$. The spectra cover a fairly broad range in energy (13–15 orders of magnitude). The burst spectral flux at 550 nm is $\approx 10^{-10}(\Gamma_0/400)^{8/3}$ ergs cm^{-2} s^{-1} eV^{-1} = $40(\Gamma_0/400)^{8/3}$ mJy, which corresponds to a magnitude $V \simeq 13 - 6.7 \log(\Gamma_0/400)$.

We can now estimate the effect of approximation (5) above (mixed RS-FS combinations in the IC spectrum are neglected), using the previous equations for the minimum electron Lorentz factor behind each shock and equations (10) and (12). The energy (in the laboratory frame) of the SY-FS photons that would be upscattered by post-RS electrons with $\gamma_{m,\mathrm{RS}}$ at the limit between the Thomson and KN regimes is $E_{\mathrm{KN}}^{\mathrm{RS}\leftarrow\mathrm{FS}} = (m_e c^2/\gamma_{m,\mathrm{RS}})\Gamma \simeq 1 f_\kappa^{-1}(\Gamma_0/400)$ MeV. Equation (12) and Figure 1 show that there are SY-FS photons that are less energetic than $E_{\mathrm{KN}}^{\mathrm{RS}\leftarrow\mathrm{FS}}$. Therefore, because of approximation (5), a fifth component of the spectrum (SY-FS photons IC scattered in the RS) is neglected. This component would have a peak below $E_{\mathrm{KN}}^{\mathrm{RS}\leftarrow\mathrm{FS}}\gamma_{m,\mathrm{RS}}^2 \simeq 10 f_\kappa(\Gamma_0/400)$ GeV if $E_{\mathrm{KN}}^{\mathrm{RS}\leftarrow\mathrm{FS}} < E_p^{\mathrm{SY,FS}}$, or at $E_{\mathrm{IC}}^{\mathrm{RS}\leftarrow\mathrm{FS}} = E_p^{\mathrm{SY,FS}}\gamma_{m,\mathrm{RS}}^2 \simeq 10 f_\kappa^4 \lambda_B^{1/2} n_0^{1/2}(\Gamma_0/400)^4$ GeV if $E_{\mathrm{KN}}^{\mathrm{RS}\leftarrow\mathrm{FS}} > E_p^{\mathrm{SY,FS}}$. The energy of the SY-RS photons that would be upscattered by FS electrons with $\gamma_{m,\mathrm{FS}}$ in a mild KN regime is $E_{\mathrm{KN}}^{\mathrm{RS}\rightarrow\mathrm{FS}} = (m_e c^2/\gamma_{m,\mathrm{FS}})\Gamma \simeq 0.8 f_\kappa^{-1}$ keV. Equation (10) and Figure 1 show that there are SY-RS photons at energies lower than $E_{\mathrm{KN}}^{\mathrm{RS}\rightarrow\mathrm{FS}}$. Approximation (5) does not take into account a sixth component of the spectrum (SY-RS photons IC scattered in the FS) that would appear at $E_{\mathrm{IC}}^{\mathrm{RS}\rightarrow\mathrm{FS}} = E_p^{\mathrm{SY,RS}}\gamma_{m,\mathrm{FS}}^2 = E_{\mathrm{IC}}^{\mathrm{RS}\leftarrow\mathrm{FS}}$. It can be shown that the cooling of FS electrons with $\gamma_{m,\mathrm{FS}}$ through this kind of scattering is less efficient than through SY emission. Therefore, the numerical results do not take into account the mixed components for IC scattering, and they underestimate the burst flux in the lower energy part of the IC-FS components shown in Figure 1. Fortunately, the flux in the most important energy range (the BATSE window) is affected very little. Otherwise, the intensity of the IC component, relative to the SY emission from each shock, as shown in Figure 1, is consistent with the previous estimations (eqs. [16], [17], and [18]).

The peak energy E_p of the spectra shown in Figure 1 passes through the BATSE window as Γ_0 is increased from 100 to 800. As expected, higher Lorentz factors lead to harder spectra (see Fig. 1 legend). This can be also seen using the hardness ratio HR_{32}, defined as the ratio of counts in the third BATSE channel (100–300 keV) to that of the second channel (50–100 keV): $\mathrm{HR}_{32}(\Gamma_0 = 100, \gamma_M/\gamma_m = 100) = 0.46$ ($T_b \simeq 500$ s), $\mathrm{HR}_{32}(\Gamma_0 = 200) = 0.50$ ($T_b \simeq 100$ s), $\mathrm{HR}_{32}(\Gamma_0 = 400) = 0.80$ ($T_b \simeq 10$ s), and $\mathrm{HR}_{32}(\Gamma_0 = 800) = 0.98$ ($T_b \simeq 2$ s). Figure 2 shows the SY-RS spectra obtained for a fixed $\Gamma_0 = 400$ and combinations of parameters (n; λ_B, κ) in which only one parameter is changed relative to the "standard" combination (1 cm^{-3}; 1, 1), showing the effect produced by each parameter and allowing comparison with the spectral peaks given by equation (12). The hardness ratios for the new spectra are $\mathrm{HR}_{32}(0.1; 1, 1) = 0.62$, $\mathrm{HR}_{32}(1; 0.1, 1) = 0.62$, and $\mathrm{HR}_{32}(1; 1, 0.1) = 0.43$.

The hardness ratio range allowed by the model is less wide than the range of E_p generated by the values of Γ_0 considered, and it is useful to compare these ratios with those of the observed bursts. The HR_{32} values above are consistent with those presented by Paciesas et al. (1992) and comparable to those found by Nemiroff et al. (1994), Mitrofanov et al. (1996), and Kouveliotou et al. (1993). According to the latter, the average HR_{32} is 0.87 for bursts with $T_b > 2$ s. The hardness ratios HR_{43} of the simulated bursts range from 0.2 to 0.4 for $200 < \Gamma_0 < 400$ (10 s $< T_b <$ 100 s) and are $\simeq 0.6$ for $\Gamma_0 = 800$, which is in good agreement with the values calculated by Dezalay et al. (1992). For the bursts shown in Figures 1 and 2, the ratio $\mathrm{HR}_{34,12}$ of the photon fluxes in channels 3 and 4 (above 100 keV) and in channels 1 and 2 (25–100 keV) is between 0.25 and 0.65, which is lower than the hardness ratios calculated by Bhat et al. (1994): $0.3 < \mathrm{HR}_{34,12} < 1$. It is also important to compare the low- and high-energy spectral indices α and β, as defined by Band et al. (1993), with observations: α is the asymptotic limit of the slope of the photon spectrum $C_E = dN_\gamma/dE$ at arbitrarily low energy, i.e., $C_E \propto E^\alpha \exp(-E/E_0)$, and β is the slope of C_E at energies higher than the spectral peak E_p ($C_E \propto E^\beta$). For the $\Gamma_0 = 400$ and $\Gamma_0 = 800$ spectra shown in Figure 1, the spectral indices α obtained

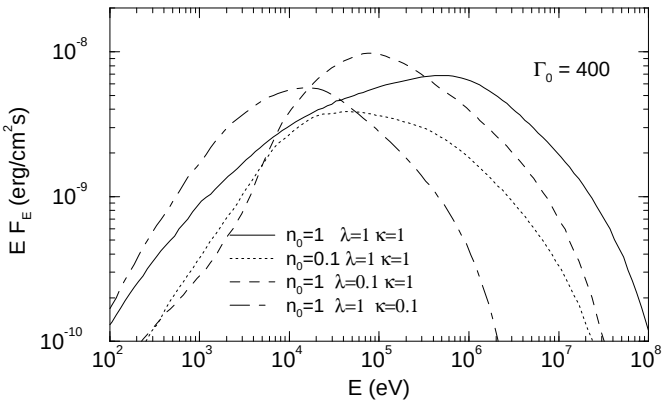

FIG. 2.—SY spectra from the FS for different sets of parameters (n_0; λ_B, κ). $E_0 = 10^{51}$ ergs, $\Gamma_0 = 400$, $D = 10^{28}$ cm, $\gamma_M/\gamma_m = 10$, and $p = 3$. $E_p(1; 1, 1) = 500$ keV; $E_p(0.1; 1, 1) = 45$ keV; $E_p(1; 0.1, 1) = 75$ keV, and $E_p(1; 1, 0.1) = 17$ keV.

from fits of spectra below E_p, using the Band function, are -1.8 and -1.6, respectively. The high-energy spectral indices for the same initial Lorentz factors are -2.9 and -2.8. These values are consistent with those found by Band et al. (1993): $-1.5 \leq \alpha \leq 0$ and $-3 \leq \beta \leq -1$. The expected analytic value of α is -1.5 (integrated spectrum of SY radiation from cooling electrons), while that of β is $-(1 + p/2) = -2.5$ (the spectrum of SY radiation from a steady-state distribution of electrons with continuous power-law injection). The slightly lower values of the indices obtained numerically result from the continuous deceleration of the FS, leading to a progressive spectral softening through decreasing magnetic field, Doppler blueshift factor, and random Lorentz factor of injected electrons. The increased steepness of the SY-FS spectra shown in Figure 1 below ~ 1 keV is due to IC scattering in the Thomson or mild-KN regimes, as predicted by equation (14).

A spectral evolution of GRBs from hard to soft has been observed by many authors (e.g., Norris et al. 1986; Mitrofanov et al. 1996; Band et al. 1992; Bhat et al. 1994; Ford et al. 1995). Figure 3 shows the light curve and temporal evolution of the spectrum resulting from a simulation with constant parameters λ_B and κ. A substantial fraction (60%) of the burst radiation falls within BATSE channels 1–4. The burst light curve exhibits a sharp rise and a slow decay, during which the flux is well approximated as a power law: $F \propto T^{-1.2}$. The bottom graph shows the burst's hard-to-soft spectral evolution: the hardness ratio HR_{32}, the mean energy E_m in the BATSE channels 1–4 (defined as the ratio of the energetic flux and photon flux in this band), and the peak energy E_p decrease monotonically during the burst (see Fig. 3 legend). During the light-curve decay ($T \geq 3$ s), these spectral parameters can be approximated by power laws in T: $HR_{32} \propto T^{-0.1}$, $E_m \propto T^{-0.2}$, and $E_p \propto T^{-1.2}$ (similar indices describe the spectral evolution of the other bursts shown in Figs. 1 and 2). The peak flux and spectrum of this burst show that its peak photon flux in the BATSE window is of order 0.1 γ cm^{-2} s^{-1}, corresponding to a weak burst. This is in part caused by the conservative choice of $E_0 = 10^{51}$ ergs over 4π sr and to the almost maximal luminosity distance $D = 10^{28}$ cm $\simeq 10^{10}$ lt-yr in this example. Beaming of the fireball in a solid angle of less than 1 sr would easily boost the peak photon flux of this burst above 1 γ cm^{-2} s^{-1}.

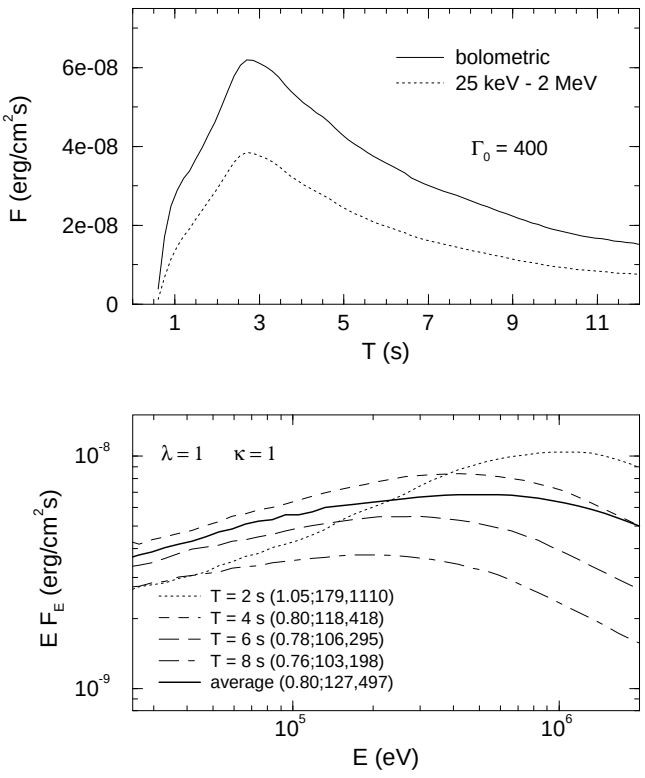

FIG. 3.—Light curve (*top*) and spectral evolution (*bottom*) for $E_0 = 10^{51}$ ergs, $n = 1$ cm^{-3}, $\Gamma_0 = 400$, $D = 10^{28}$ cm, $\lambda_B = 1$, and $\kappa = 1$. The detector time T is measured from the moment of the explosion that generated the fireball. 60% of the burst energy arrives at detector in the BATSE channels 1–4. The legend of the bottom graph indicates the hardness ratio HR_{32}, the mean energy E_m in keV in the BATSE window, and the spectral peak E_p in keV (in this order), at different moments and for the averaged spectrum.

In an efficient burst the synchrotron cooling time of the FS electrons is much shorter than the hydrodynamic timescale. Consequently, most of the burst radiation is emitted by the leading edge of the expanding shell of shocked fluid from a region that is $t_{\rm dec} \simeq 10^3$–$10^4 t^{\rm SY}$ times thinner than the shell containing all the shocked fluid. At detector time T corresponding to t, the observer is not receiving radiation from this very thin subshell, but from a very elongated ellipsoid (see Rees 1966) of semimajor axis $\sim r_{\rm dec}$. Consequently, the detector receives radiation that was emitted at times spread over $\sim t_{\rm dec}$, which means that the spectrum and light curve reflect the long timescale variations of the burst physical parameters, while all features arising from short timescale variations are well mixed and less distinguishable. The Lorentz factor $\Gamma(t)$ of the shocked fluid is monotonously decreasing; therefore, at constant energy release parameters κ and λ_B (relaxation of this assumption is considered in § 4), the spectral evolution of the burst shows only the time evolution of $\Gamma(t)$. Thus, the hard-to-soft spectral evolution shown in Figure 3 purely results from the deceleration of the radiating fluid.

4. BURST SUBSTRUCTURE

We further test the ability of the blast wave model to accommodate some of the more frequently observed features of spectral evolution in bursts that exhibit individual pulses, although exceptions from these rules are not uncommon.

1. The spectrum hardens before an intensity spike and softens while the photon flux is still increasing (Mitrofanov et al. 1992b; Kouveliotou et al. 1992; Band et al. 1992; Bhat et al. 1994; Ford et al. 1995).
2. The hardness of successive spikes decreases (Norris et al. 1986; Band et al. 1992; Ford et al. 1995).
3. Pulses peak earlier in the higher energy bands (Norris et al. 1986; Kouveliotou et al. 1992; Norris et al. 1996).
4. Pulses exhibit faster rises at higher energies and longer decays at lower energies (Norris et al. 1996), so peaks are shorter at higher energy (Link, Epstein, & Priedhorsky 1993; Fenimore et al. 1995; Mitrofanov et al. 1996).

Since the flow Lorentz factor of the radiating shocked fluid is monotonously decreasing, the simple kinematics of this fluid cannot, by itself, produce spectra showing increasing hardness or light curves containing peaks (assuming spherical symmetry), so departures from this simplest case need to be considered in order to explain such features.

4.1. *Temporal Variability from EM Inhomogeneities*

The pulses that are observed in bursts could have some relation to fluctuations in the EM density, with denser EM blobs leading to a more intense release of energy. In this scenario, the spherical symmetry is lost, and a three-dimensional hydrodynamic code is required to perform numerical simulations. The following is a purely analytical model of the situation. The duration of each pulse is determined by the following three factors:

1. The projection of the shocked inhomogeneity on the line of sight toward the center of explosion, determined by (*a*) the laboratory frame thickness δr of the overheated radiating region, and (*b*) the angle $\delta\theta = R/r$ subtended by the shocked blob around its position θ on the spherical cap from which the observer receives radiation, where R is the radius of the unshocked blob, assumed to be spherical. R should be less than the radius $r/\Gamma \sim r_{\rm dec}/\Gamma \simeq 3 \times 10^{13} n_0^{-1/3}(\Gamma_0/400)^{-5/3}$ cm of the visible spherical cap, or the pulse would last as long as the whole burst.

2. The time it takes to sweep up the entire inhomogeneity.

3. The laboratory frame duration of the energy release $\delta t \sim t^{\rm SY}$ (eq. [20]).

The contributions of these factors to the pulse duration are (1*a*) $\Delta T_{\delta r} = \delta r/c \sim 2R/\Gamma_b^2 c$, (1*b*) $\Delta T_{\delta\theta} = 2\theta R/c$; (2) $\Delta T_R = R(\Gamma_b^{-2} + \theta^2)/c$; and (3) $\Delta T_{\delta t} = \delta t(\Gamma_b^{-2} + \theta^2)/2$, where Γ_b is the flow Lorentz factor of the shocked blob, which we will approximate by the Lorentz factor Γ of the rest of the shocked EM, although it must be lower, because the inhomogeneity is denser. In calculating $\Delta T_{\delta r}$ above, we used the fact that in the laboratory frame, the shocked blob material is $\sim\Gamma_b^2$ times denser than before the shock, therefore $\delta r \sim 2R/\Gamma_b^2$. Since $\Delta T_{\delta r}$ and ΔT_R are of order $R/\Gamma^2 c$, and $\Delta T_{\delta\theta} \approx R/\Gamma c$, it follows that $\Delta T_{\delta r}, \Delta T_R \ll \Delta T_{\delta\theta}$. Furthermore, if $R \gtrsim 10^{10}\kappa^{-1}\lambda_B^{-1} n_0^{-1}(\Gamma_0/400)^{-3}$ cm, then $\Delta T_{\delta t}$ can be neglected, relative to $\Delta T_{\delta\theta}$. Thus, for $10^{-3}\kappa^{-1}\lambda_B^{-1} n_0^{-1}(\Gamma_0/400)^{-3}$ AU $\lesssim R \lesssim 1 n_0^{-1/3}(\Gamma_0/400)^{-5/3}$ AU (assumption [1]), $\Delta T_{\delta\theta}$ determines the duration of the pulse. If R is less than the lower limit set above, then one has to consider the contribution of the cooling time to the pulse duration. If R is above the upper limit, then the pulse duration is comparable to T_b, and it would be impossible to have bursts with more than a few pulses.

In order to derive the distribution $P(\Delta T)$ of the durations of pulses in individual bursts, we assume that the comoving photon number spectrum of the radiation emitted by each blob is a power law $dN_\gamma = C\varepsilon^{-\sigma}\, d\varepsilon$ (assumption [2]) over a range in energies $\varepsilon_{\rm min}$–$\varepsilon_{\rm max}$ wide enough that the blueshifted corresponding laboratory frame range covers the band in which observations are made for all blobs that are seen by the observer (i.e., for all inhomogeneities that produce at the detector a peak photon flux above a given threshold $C_{\rm lim}$). Thus we assume that the Doppler-shifted edges of the comoving spectrum: $E_{\rm min\,(max)}(\Gamma, \theta) = \varepsilon_{\rm min\,(max)}/[\Gamma(1 - v\cos\theta)]$, where $v = (\Gamma^2 - 1)^{1/2}/\Gamma$ is the flow velocity, satisfy $E_{\rm min} \le E_m$ and $E_M \le E_{\rm max}$ (assumption [3]), where E_m and E_M are the lower and upper edges of the observational band. If so, the peak photon flux C_p of each pulse is $C_p \propto [C/(\sigma - 1)][\Gamma(1 - v\cos\theta)]^{-\sigma-2}$. The constant C can be determined by using the fact that the total number of photons emitted per unit time in the comoving frame $\{= [C/(\sigma - 1)]\varepsilon_{\rm min}^{1-\sigma}$, if $\sigma > 1$ and $\varepsilon_{\rm min} \ll \varepsilon_{\rm max}\}$ is equal to the number of emitting electrons N_e multiplied by the number of photons emitted per unit time by each electron, which is independent of the Lorentz factor of the electron and depends only on the magnetic field B. If all blobs are identical not only in size but also in density (assumption[4]), then N_e is the same for all pulses, and therefore $C/(\sigma - 1) \propto B\varepsilon_{\rm min}^{\sigma-1}$. The minimum comoving energy $\varepsilon_{\rm min}$ of the SY photons is proportional to B and to γ_m^2, where γ_m is the minimum Lorentz factor of the electrons accelerated when the FS interacts with the EM inhomogeneity. We further assume that the parameters for energy release (κ, λ_B, γ_M/γ_m, p) are the same for all blobs (assumption [5]), so that $B \propto \Gamma$, and $C/(\sigma - 1) \propto \Gamma^{3\sigma-2}$. In the end, the peak photon flux at the detector for any pulse can be written as

$$C_p(\Gamma, \theta) = \frac{\rm const}{D^2} F_1(E_m, E_M; \sigma) F_2\left(p, \frac{\gamma_M}{\gamma_m}; \sigma\right) \times n_{\rm blob}^{1+\sigma/2}\lambda_B^{\sigma/2} f_\kappa^{2(\sigma-1)} R^3 \frac{\Gamma^{2\sigma-4}}{(1 - v\cos\theta)^{\sigma+2}}, \quad (22)$$

where F_1 and F_2 are generic notations for functions of the indicated variables, and $n_{\rm blob}$ is the density of the inhomogeneity.

The condition $C_p(\Gamma, \theta) \ge C_{\rm lim}$ determines which blobs yield pulses that are detectable, provided that the kinematics $\Gamma(\Gamma_0, r)$ of the shell during the deceleration phase and the spatial distribution $n_b(r)$ of the blobs are known. For an adiabatic interaction, $\Gamma(r) \propto r^{-3/2}$. Numerically, we found that $\Gamma(r) = 1/2\Gamma_0(r/r_{\rm dec})^{-3/2}$ is a good approximation. The number density of the EM inhomogeneities is considered to be a power law: $n_b(r) \propto r^{-m}$ (assumption [6]). Thus, the homogeneous distribution is the particular case $m = 0$. Based on these assumptions, one can determine, for any shell position r, the maximum angle $\theta_{\rm max}(r)$ relative to the line of sight toward the center of explosion for which $C_p[r, \theta_{\rm max}(r)] = C_{\rm lim}$ and integrate over r and θ to find the pulse duration distribution. Figure 4 (*top*) shows this distribution for a representative set of parameters (R, Γ_0, m, σ, $C_{\rm max}/C_{\rm lim}$), where the last parameter is a measure of how bright the pulse is from a blob located at ($r = 1r_{\rm dec}$, $\theta = 0$), relative to the detection threshold. The same figure allows one to assess the importance of each parameter: $P(\Delta T)$ is rather insensitive to Γ_0 and depends strongly on R. The lack of correlation with the initial Lorentz factor is due to the fact that $\theta_{\rm max}(r)$ is weakly dependent on Γ_0, while the strong correlation with the blob size is clearly implied by $\Delta T_{\delta\theta} \propto R$. If the observed burst substructure is caused by EM inhomogeneities, and if the assumptions made here are not far from reality, then the latter correlation could be used to infer the typical size of these inhomogeneities from observations. As expected, if the pulse detection threshold is decreased, longer pulses are seen, as more blobs at larger angles become brighter than $C_{\rm lim}$.

The statistics of pulses in a set of bursts can be derived by convolving the pulse duration distribution for individual bursts with the distribution $P(\Gamma_0)$ of the initial Lorentz factors of the shells that generated the bursts in that set. For this, we assume that $P(\Gamma_0) \propto \Gamma_0^{\nu}$ for $\Gamma_{\rm min} \le \Gamma \le \Gamma_{\rm max}$ (assumption [7]), that all shells run into the same EM (assumption [8]), and that all bursts distances are the same (assumption [9]). Such pulse duration distributions are shown in Figure 4 (*bottom*) for $\Gamma_{\rm min} = 200$ and $\Gamma_{\rm max} = 800$. $C_{\rm max}$ (as defined above) for $\Gamma_0 = 200$ was chosen to be 10 times larger than $C_{\rm lim}$; this determines $C_{\rm max}$ for any other Γ_0. It can be seen that $P(\Delta T)$ is not strongly dependent on

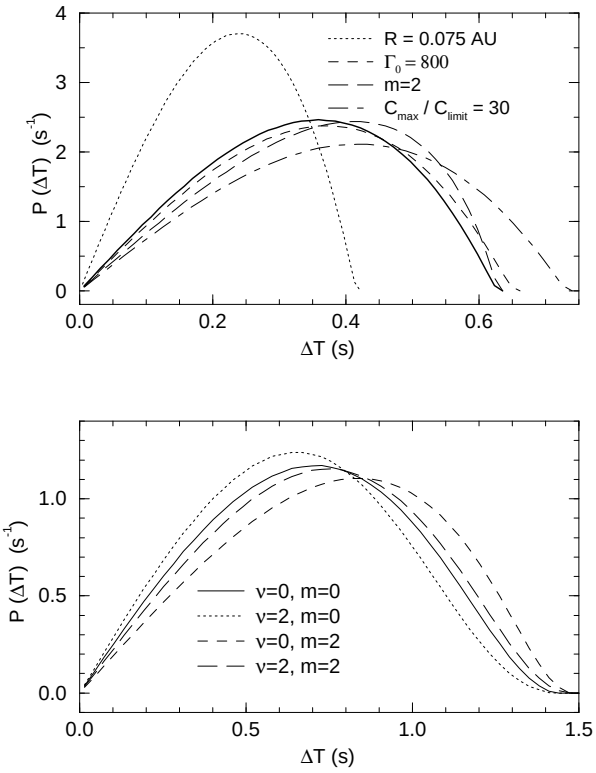

FIG. 4.—Burst substructure from EM inhomogeneities. *Top*: Pulse duration distribution for individual bursts. The solid curve is for $R = 0.1$ AU, $\Gamma_0 = 400$, $\sigma = 2$, $m = 0$ (homogeneous distribution of blobs), and a pulse detection threshold $C_{\rm limit} = C_{\rm max}/10$, where $C_{\rm max}$ is the photon flux that a blob located on the line of sight toward the center of explosion and at $r = 1r_{\rm dec}$ yields at the detector. Other distributions shown are for the same set of parameters, except that indicated in the legend. *Bottom*: Duration distribution for a set of bursts. The combinations of initial Lorentz factor distribution and spatial distribution of the EM inhomogeneities are indicated in the legend. Parameters: $R = 0.1$ AU, $\Gamma_{\rm min} = 200$, $\Gamma_{\rm max} = 800$, $\sigma = 2$, and $C_{\rm max}(\Gamma_{\rm min})/C_{\rm limit} = 10$.

the parameters v and m. Thus, it is possible to estimate the size of the blobs by using durations of pulses in different bursts, as R remains the parameter that most affects the pulse duration distribution. The pulse decomposition performed by Norris et al. (1996) shows that for the brightest bursts, ΔT is between 0.1 s and a few seconds, and therefore that R must be of order 0.1 AU.

If radiation is emitted not only from the higher density blobs, but also from the rest of the EM, the effect of a more intense emission of radiation from a blob, combined with a stronger decrease of the flow Lorentz factor induced by the same blobs, is likely to lead to a shallow peak. In other words, the radiating power of the source is increased, but, at the same time, the radiation received by the detector is more stretched out in time than the radiation emitted before and after, ironing out the peak. We are thus forced to assume that only the blobs emit significant radiation (perhaps because of an enhanced magnetic field). In this case, however, a new difficulty arises: as Sari & Piran (1997) pointed out, if pulses do not overlap significantly, the upper bound on the size of the emitting blobs set by the observed pulse durations limits the fraction of the area covered by these blobs on the spherical cap that is visible to the observer to about 1%, leading to a low burst efficiency. (A higher efficiency can be reached if the number of blobs is large enough to cover the entire spherical cap visible to the observer, but the pulses then lose their individuality, producing a single-hump burst.) In order to explain the observed burst fluences, one has then to assume that the ejecta is beamed into a fraction that is $\frac{1}{100}$ of the full sky, and that almost 99% of the initial energy is not released as gamma rays or is lost adiabatically. Thus, in principle, this explanation for a complicated pulse structure can work if the ejecta is in a jet, without increasing the total energy to above 10^{51} ergs, if 99% of this energy can go undetected.

4.2. *Temporal Variability from Energy Release Fluctuations*

To explore the limits of the ability of external shock models to generate pulses, we consider a second, idealized scenario, in which the burst substructure results from fluctuations in the parameters λ_B and κ that characterize the release of the internal energy stored in the shocked gas. Here we consider the case in which κ is constant in time, and we assume a variable magnetic field. A time-varying κ should have a similar effect on the cooling timescale ($t^{\rm SY} \propto \lambda_B^{-1}\kappa^{-1}$), but a stronger one on the spectrum ($E_p^{\rm SY,RS} \propto \lambda_B^{1/2}\kappa^2$). If the magnetic fields are such that (1) at their maximum value, the burst radiates mainly in the BATSE window, and (2) at minimum value, $t^{\rm SY} > t_{\rm dec}$ (the source is in a γ-quiet phase), then equations (12) and (20) show that λ_B must vary by more than 4 orders of magnitude: $\lambda_{B,\rm min} \lesssim 10^{-4}$ and $\lambda_{B,\rm max} \lesssim 1$; i.e., the magnetic field must vary by at least 2 orders of magnitude. We do not speculate here on the nature of the microscopic process that could produce such fluctuations of more than 2 orders of magnitude in the magnetic field strength over timescales that should be shorter than $0.1t_{\rm dec}$; we remark only that plasma dynamo mechanisms that build up the field to a fraction of the equipartition value could plausibly result in such field variations. In the presence of such variations multipeaked bursts are obtained, as shown below.

In Figure 5 we show a burst with two peaks, resulting from a relatively large-scale variation of λ_B (see Fig. 5*a*, *inset*). The spectral evolution is shown with open symbols in Figure 5*a*: E_m is decreasing during the first peak ($T_{p,1} \simeq 1$ s), then increases and peaks around $T = 2$ s, approximately 1 s before the photon flux and energetic flux peaks ($T_{p,2} \simeq 3$ s), and monotonously decreases through the remainder of the burst. The hardness ratio $\rm HR_{32}$ shows the same behavior. The monotonous spectral softening of the burst during the first peak is caused by the deceleration of the shocked fluid and by the fact that this simulation was started from $0.5t_{\rm dec}$. Thus, the radiation emitted by the fluid moving at angles $\sim\Gamma^{-1}$ (relative to the observer) prior to $t = 0.5t_{\rm dec}$ is not accounted for, resulting in an artificial softening of the spectrum during the first peak that obscures the spectral evolution expected from a variable magnetic field. This is not the case with the spectral evolution during second peak, which shows clearly the second λ_B pulse. The duration and temporal symmetry of each peak can be characterized through the rise and fall times $T_R = \int_0^{T_p} dT f(T)$ and $T_F = \int_{T_p}^{T_b} dT f(T)$, where $f(T)$ is the photon (or energetic) flux normalized to its maximum value (reached at the peak time T_p), and through the time-asymmetry ratio $A = T_F/T_R$. T_p, the pulse duration $\Delta T = T_R + T_F$, and the ratio A are given for each peak in the legends of Figures 5*c* and 5*d*. Note that both pulses are narrower and peak earlier at higher energies, features known to occur in observed GRBs. The rise and fall times of the pulses decrease with energy, but their time asymmetries show opposite trends: the first pulse appears more sym-

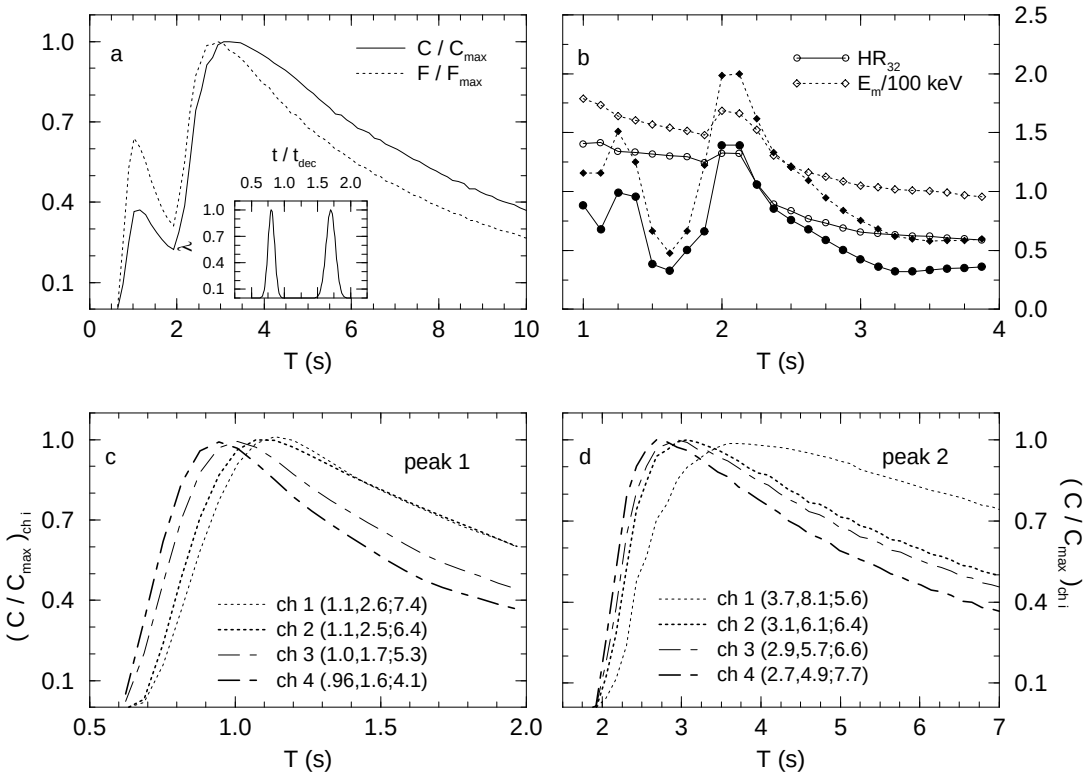

FIG. 5.—Burst substructure from energy release fluctuations. Time history, spectral evolution, and pulses' shapes in BATSE channels 1–4 for $E_0 = 10^{51}$ ergs, $n = 1$ cm^{-3}, $\Gamma_0 = 400$, $D = 10^{28}$ cm, $\kappa = 1$, and time variable λ_B (*light curve*), shown in the inset of (*a*). (*b*) Hardness ratio HR_{32} and mean energy E_m in the BATSE channels 1–4. Open symbols are for an isotropic emission in the comoving frame, filled symbols are for an anisotropic case: radiation emitted within $4\pi/17$ sr of the radial flow direction. Note that the second peak ($T_p \simeq 3$ s) shows a stronger increase in spectral hardness in the latter case, and that in both cases the maximum spectral hardness occurs ~ 0.5–1 s before the intensity peak. (*c*) The first peak, as seen in each BATSE channel. (*d*) The second peak in the same bands. Fluxes in (*c*) and (*d*) are normalized to the peak value in that channel. Legends in (*c*) and (*d*) give the peak time, duration (sum of the rise and fall times, as defined in the text), and time-asymmetry ratio of each peak, respectively, in each BATSE channel.

metric at higher energies, while the second is more symmetric at lower energies. In $\log \Delta T - \log \bar{E}$, where $\bar{E}$ is the geometrical mean of the low and high edges of the four BATSE channels, the two pulses appear to be relatively scattered from a straight line; nevertheless, if a power law is fitted, $\Delta T \propto E^{-0.20}$. If the pulse FWHM is used, then $\Delta T_{\rm FWHM} \propto E^{-0.24}$. A clearer power-law dependence is found for the single-pulse burst shown in Figure 3: ΔT, $\Delta T_{\rm FWHM} \propto E^{-0.15}$. Norris et al. (1996) decomposed 41 bright GRBs into pulses and found that the average FWHM of the pulses varies with energy as $E^{-0.33}$ if only the separable pulses are used and as $E^{-0.38}$ for all the pulses in the analyzed bursts. Therefore, the pulse duration-energy anticorrelation of our simulated bursts is somewhat weaker than observed. The second peak in Figure 5*a* is slightly more time asymmetric than the first peak (in BATSE channels 1–4: $A_1 = 5.0$ and $A_2 = 5.4$); it is also wider, more shifted to later times at lower energies (Fig. 5*c* vs. 5*d*), and spectrally softer (as shown by HR_{32} in Fig. 5*b*). These are exactly the relative features observed by Norris et al. (1996) in their pulse decomposition analysis. The blast wave model reproduces the increase in the burst hardness before an intensity peak, but the simulated spectral hardening is weaker than what is observed.

If radiation is emitted isotropically in the comoving frame (as would be the case for a turbulent magnetic field), then the observer receives radiation mainly from portions of the fluid moving at angles $\lesssim \Gamma^{-1}$ relative to the line of sight. Light emitted by such a spherical cap at time t is spread in detector time T over $\Delta T(t) = r(t)/2\Gamma^2(t)$, where $r(t)$ is the radial coordinate of the cap. Since the flow is ultrarelativistic, $r(t) \simeq ct$, and thus $\Delta T(t) \lesssim T_b$ (from eq. [2]). This means that any instantaneous event that occurs in the spherical shell is seen by the observer as smeared over a good fraction of the burst. Pulselike emission of radiation and spectral features resulting from a change in the fluid physical parameters are ironed out very efficiently by sampling over the entire opening angle of the region seen by the observer. This naturally suggests that, if spherical symmetry in the laboratory frame is maintained, the angular opening of the cap from which the detector receives radiation must be less than Γ^{-1}, in order to reduce the blending of the temporal and spectral features arising from fluctuations in the burst physical parameters. This could happen if the radiation, instead of being emitted isotropically in the comoving frame, is beamed along the radial direction of fluid motion. If this radiation is concentrated in two cones of solid angles $2\pi(1 - \mu_{\rm co})$ sr around the radius vector, then the observer receives radiation from a cap of angular opening $[(1 - \mu_{\rm co})/(1 + \mu_{\rm co})]^{1/2}\Gamma^{-1} < \Gamma^{-1}$.

The effect of such an anisotropic emission can be assessed from Figure 6. As the radiation in the comoving frame is emitted within a narrower solid angle, the light curve becomes more time symmetric. Due to the monotonous spectral softening (λ_B and κ are constant, and Γ decreases), the photon flux decays more slowly than the energetic flux and is therefore more time asymmetric (see the rise and fall times given in graph legends). This figure can be compared

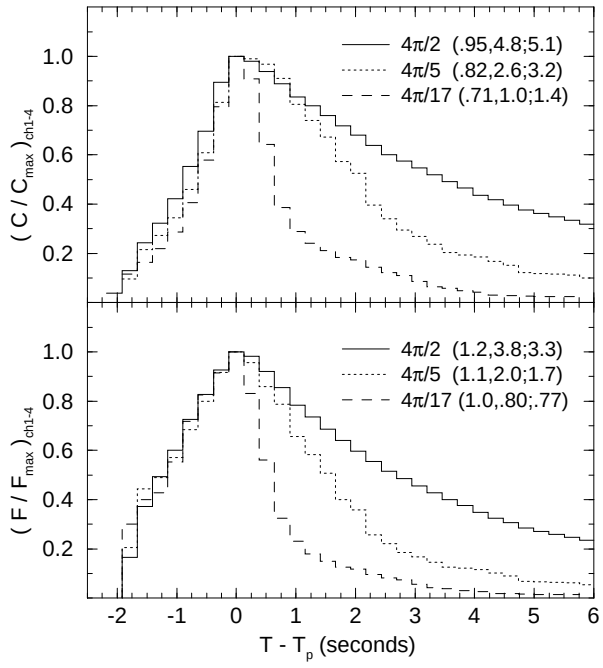

FIG. 6.—BATSE-window time histories of a burst with $\Gamma_0 = 400$ and different degrees of anisotropy of radiation emission in the comoving frame. *Solid curves*: Isotropic emission (two cones, each of $4\pi/2$ sr solid angle, corresponding to a cap of angular opening Γ^{-1} in the laboratory frame); *dotted and dashed curves*: anisotropic emission ($4\pi/5$ sr and $4\pi/17$ sr comoving frame solid angles, corresponding to $0.5\Gamma^{-1}$ and $0.25\Gamma^{-1}$ angular opening caps, respectively). Note that as the comoving frame anisotropy increases, the light curves becomes more symmetric. Legends indicate the rise and fall times and the asymmetry ratio, as defined in the text, respectively. *Top*, Photon fluxes; *bottom*, energetic fluxes. Light curves have been normalized to their peak fluxes, binned in 256 ms, and aligned at their peaks.

to similar ones, presented by Mitrofanov et al. (1996), showing the GRB "average curve of emissivity" in the BATSE channels 2 + 3. In the isotropic case, the radiation emitted by the fluid moving at large angles ($\lesssim \Gamma^{-1}$) relative to the line of sight is Doppler blueshifted by a factor $\lesssim 2$, relative to the radiation emitted by the fluid moving exactly toward the observer. This large-angle radiation arrives later at the detector, and it is mixed with the radiation emitted at later times, but from regions moving at smaller angles. As the comoving-frame solid angle in which radiation is emitted decreases, the detector receives less radiation from the fluid moving at large angles; therefore, the radiation emitted at different times is less mixed, and the spectrum reflects better the instantaneous physical conditions of the radiating fluid. For Figure 6 this means that the spectrum shows the deceleration of the shocked fluid in the anisotropic case better than in the isotropic one. This can be seen in the evolution of the three spectral parameters used thus far during the burst fall ($T > T_p$): $\mathrm{HR}_{32} \propto T^{-0.1}$, $E_m \propto T^{-0.2}$, and $E_p \propto T^{-1.2}$ in the isotropic case; $\mathrm{HR}_{32} \propto T^{-0.5}$, $E_m \propto T^{-0.7}$, and $E_p \propto T^{-2.1}$, if, in the comoving frame, the radiation is emitted within $4\pi/5$ sr around the radial direction; while, in the most anisotropic emission considered here ($4\pi/17$ sr around the direction of flow), $\mathrm{HR}_{32} \propto T^{-0.9}$, $E_m \propto T^{-1.3}$, and $E_p \propto T^{-2.7}$. During the burst fall, the Lorentz factor of the leading edge of the expanding gas (from which comes most of the radiation received by the detector if $t^{\mathrm{SY}} \ll t_{\mathrm{dec}}$) is approximately $\Gamma \propto T^{-2/3}$, which implies that the fastest possible spectral peak evolution is $E_p(\propto \Gamma^4) \propto T^{-2.7}$. Therefore, the most anisotropic case considered above yields a spectral evolution that reflects very well the deceleration of the shocked fluid. For Figure 5 the anisotropic emission allows the spectrum to show the effect of a varying λ_B better (Fig. 5*b*, *filled symbols*): note the much faster spectral softening during the first pulse and the sharp spectral hardening before the second peak.

The same type of anisotropic emission can be used to generate multipeak bursts, as is shown in Figure 7. The standard of comparison is an isotropic emission case (Fig. 7, *top*), for which the radiation coming from the source is blended into a single-hump light curve. The more anisotropic the emission is, the shorter and brighter the pulses, and the better distinguishable the individual peaks. The progressive spectral softening renders these peaks less well separated in photon flux than in energy flux, as can be seen

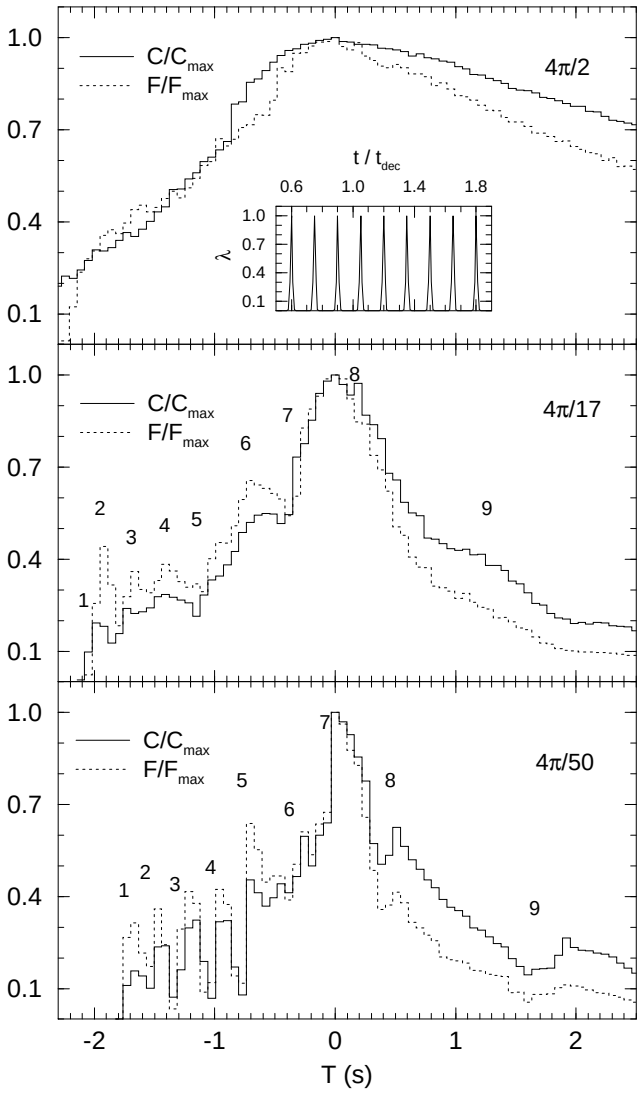

FIG. 7.—$\Gamma_0 = 400$ multipeak burst (in BATSE window) generated by a variable magnetic field (*top*, *inset*). *Top*: Isotropic emission. *Middle and bottom*: Anisotropic emission. The solid angle around the direction of motion in which the emission is confined is indicated in each graph. Note that as the degree of anisotropy increases, the peaks become more distinct. Photon and energy fluxes have been normalized at the maximum value reached during the burst, aligned at their peak times, and binned in 64 ms. Numbers indicate the expected beginning of each pulse.

in the middle graph of Figure 7. Pulses appear more distinct in the case of maximum anisotropy considered here (Fig. 7, *bottom*). If much internal energy were to accumulate in the shocked fluid between two consecutive λ_B pulses, and if most of it is radiated during a magnetic field pulse, then the observed peaks may be blended into a single one (as happens with the pairs of pulses 1 and 2, 5 and 6, and 7 and 8 in the middle graph). The pulse onset times, calculated from the time when $t^{SY} < t_{dec}$ and using the radial coordinate of the shell's leading edge, are indicated with numbers. The peak of each pulse occurs slightly later, because of the angular opening and thickness of the source. Note that later pulses are more time asymmetric than earlier ones and last longer; this is caused by the continuous deceleration of the source. A larger number of pulses can be simulated by using an even stronger comoving frame anisotropy.

5. CONCLUSION

We have discussed some features of numerically simulated GRB spectra and light curves from external shock models, paying particular attention to the expected spectral-temporal correlations and the expected degree of temporal substructure. The values of the most important model parameters (Γ_0, n; λ_B, κ) were chosen such that the burst releases an important fraction of its energy in the BATSE window. No effort was made to optimize these parameters so that the simulated bursts would mimic the observed ones, other than considering (phenomenologically) the effects of a variable magnetic field and an anisotropic emission pattern in the comoving frame for some of the models. We then compared the features of the numerical bursts with characteristics of the observed GRBs that are well established, such as the spectral hardnesses, low- and high-energy spectral indices, hard-to-soft spectral evolution, correlation between spectral hardness and intensity, pulse duration versus energy, etc. We summarize here the features of the numerically simulated model bursts:

1. Brightness and spectral hardness are correlated.

2. The bursts show a spectral hardness-duration anticorrelation: $E_p \propto T_b^{-3/2}$. The observed dependence is weaker, which could result from the variations of the energy release parameters (λ_B, κ) from one burst to another.

3. For single-pulse light curves, the photon flux in the BATSE window rises as $T^{1.6}$ and decays approximately as $T^{-1.0}$. The fall is steeper when the comoving frame emission is anisotropic.

4. The low-energy index of the averaged spectrum is $\alpha = -1.7 \pm 0.2$, which is not far from the expected value of -1.5. For $p = 3$ the high-energy index is $\beta = -2.8 \pm 0.1$, which is not far from -2.5, the theoretical value. The former index is determined by the evolution of the accelerated electrons if the spectral peak E_p is in the BATSE window, while the latter index depends upon the choice of the electron power-law index p.

5. The spectra show a general hard-to-soft evolution outside of intensity pulses. In single-hump light curves arising from isotropic comoving frame emission, the spectral evolution at $T > T_p$ is characterized by $E_p \propto T^{-1.1 \pm 0.1}$. If in the comoving frame radiation is emitted preferentially on the radial direction of motion, the spectral evolution is faster.

6. The peak (or break) energy E_p increases with intensity during a pulse, but peaks earlier. The mean energy E_m in the BATSE window and the hardness ratio HR_{32} (or similar ones) show a similar trend. The increase in the burst hardness before an intensity peak is stronger in the case of anisotropic emission.

7. Earlier pulses are harder and have a more time-symmetric profile at higher energies. Later pulses may show an opposite trend: more symmetry at lower energies.

8. Pulses peak earlier and are shorter in higher energy bands than at lower energies. Numerically, we found that the pulse duration scales as $E^{-0.20 \pm 0.05}$, which is a weaker dependence than observed ($E^{0.3-0.4}$). We must recognize here that, taking into account some of the approximations made, the BATSE channels are relatively narrow for the accuracy of our simulations, so the calculated pulse duration versus energy dependence can be considered to be satisfactorily close to what is observed.

9. The angular opening of the region from which the observer receives radiation limits the number of separate pulses to very few. A larger number of pulses results if radiation is not emitted isotropically in the comoving frame. Later pulses are more time asymmetric than earlier ones, and they last longer, if they result from a periodic variation of the source radiating power.

The above list of burst characteristics is in agreement with, or at least close to, what is observed. It is worth noting that the brightness-duration anticorrelation induced by the fireball Lorentz factor Γ_0 will be weakened by any dispersion in some of the other parameters involved in the model, such as the distance D to the burst, the source initial kinetic energy E_0, and the energy release parameters (κ, λ_B), which could explain why this anticorrelation is controversial or, at best, very weak.

Another major observational feature against which to contrast models is the bimodality in duration distribution. One reason why this is expected in external shock models of GRBs (Sari et al. 1996) is related to the limited energy range in which BATSE is sensitive: significant energy arrives at the detector in the BATSE window either from the FS, in the case of the long bursts, or from the RS, in the case of the short bursts, but from neither of these shocks for bursts with durations $T \simeq 2$ s. Moreover, such different burst origins can explain the lack of a duration-brightness anticorrelation: the RS is less efficient than the FS in converting the fireball kinetic energy into gamma rays, diminishing the brightness of the short burst. In our model the RS is always mildly relativistic and radiates inefficiently (i.e., at energies outside the BATSE window). If the expanding shell thickness increases faster than we considered, before its deceleration becomes important, the density of the colliding shell can be small enough to lead to the formation of a more relativistic RS. The electron Lorentz factor can be further boosted if an injection fraction well below unity is assumed. In this case the burst duration bimodality would be reproduced numerically. A different explanation (Mészáros & Rees 1993) for a bimodal duration distribution may be that shorter GRBs arise from events in a relatively dense external environment (the external shocks occur in the progenitor's own preejected wind or in a denser galactic disk environment) while longer GRBs could be caused by events in a much lower density environment (e.g., the object has moved out of its own pre-ejected wind, or it has escaped the galactic disk).

In summary, the external shock or blast wave model can

explain the spectral features and correlations of most bursts. It can also explain the time histories of bursts that have a simple structure (up to 4–8 pulses), if the magnetic field is variable, and if the comoving emissivity is appreciably anisotropic. It is difficult to see how this could be extended to fit bursts with more than 8–10 pulses as well. There is no difficulty in explaining the latter in outflows with "internal" shocks (e.g., Rees & Mészáros 1994), which are expected to have similar spectral properties, without limitations on the degree of variability. Nevertheless, external shock models show a remarkable degree of qualitative agreement with a large range of medium- to long-timescale spectral and temporal correlations exhibited by the GRB data. This suggests either that external shocks may be responsible for part of the emission of a GRB, or else that a substantial subset of bursts (i.e., the less variable ones) may be ascribed to external shock events.

This research has been supported in part through NASA grant NAG 5-2362.

REFERENCES

Band, D., et al. 1992, in AIP Conf. Proc. 265, Gamma-Ray Bursts, ed. W. S. Paciesas & G. J. Fishman (New York: AIP), 169
———. 1993, ApJ, 413, 281
Bhat, P. N., et al. 1994, ApJ, 426, 604
Blandford, R. D., & McKee, C. F. 1976, Phys. Fluids, 19, 1130
Briggs, M. S., et al. 1996, ApJ, 459, 40
Dezalay, J.-P., Barat, C., Talon, R., Sunyaev, R., Terenkhov, O., & Kuznetsov, A. 1992, in AIP Conf. Proc. 265, Gamma-Ray Bursts, ed. W. S. Paciesas & G. J. Fishman (New York: AIP), 304
Fenimore, E. E., in't Zand, J. J. M., Norris, J. P., Bonnell, J. T., & Nemiroff, R. J. 1995, ApJ, 448, L101
Ford, L. A., et al. 1995, ApJ, 439, 307
Horack, J. M., & Emslie, A. G. 1994, ApJ, 428, 620
Kouveliotou, C., Norris, J. P., Fishman, G. J., Meegan, C. A., Wilson, R. B., & Paciesas, W. S. 1992, in AIP Conf. Proc. 265, Gamma-Ray Bursts, ed. W. S. Paciesas & G. J. Fishman (New York: AIP), 299
Kouveliotou, C., Meegan, C. A., Fishman, G. J., Bhat, N. P., Briggs, M. S., Koshut, T. M., Paciesas, W. S., & Pendleton, G. N. 1993, ApJ, 413, L101
Link, B., Epstein, R. I., & Priedhorsky, W. C. 1993, ApJ, 408, L81
Mallozzi, R. S., Paciesas W. S., Pendleton, G. N., Briggs, M. S., Preece, R. D., Meegan, C. A., & Fishman, G. J. 1995, ApJ, 454, 597
Meegan, C. A., Fishman, G. J., Wilson, R. B., Paciesas, W. S., Pendleton, G. N., Horack, J. M., Brock, M. N., & Kouveliotou, C. 1992, Nature, 355, 143
Mészáros, P., Laguna, P., & Rees, M. J. 1993, ApJ, 415, 181
Mészáros, P., & Rees, M. J. 1993, ApJ, 405, 278
Mészáros, P., Rees, M. J., & Papathanassiou, H. 1994, ApJ, 432, 181
Mitrofanov, I. G., Chernenko, A. M., Pozanenko, A. S., Briggs, M. S., Paciesas, W. S., Fishman, G. J., Meegan, C. A., & Sagdeev, R. Z. 1996, ApJ, 459, 570
Mitrofanov, I. G., et al. 1992a, in AIP Conf. Proc. 265, Gamma-Ray Bursts, ed. W. S. Paciesas & G. J. Fishman (New York: AIP), 163
———. 1992b, in Gamma-Ray Bursts, ed. C. Ho, R. I. Epstein, & E. E. Fenimore (Cambridge: Cambridge Univ. Press), 209
Nemiroff, R. J., Norris, J. P., Bonnell, J. T., Wickramasinghe, W. A. D. T., Kouveliotou, C., Paciesas, W. S., Fishman, G. J., & Meegan, C. A. 1994, ApJ, 435, L133
Norris, J. P., Bonnell, J. T., Nemiroff, R. J., Scargle, J. D., Kouveliotou, C., Pacieses, W. S., Meegan, C. A., & Fishman, G. J. 1995, ApJ, 439, 542
Norris, J. P., Nemiroff, R. J., Bonnell, J. T., Scargle, J. D., Kouveliotou, C., Paciesas, W. S., Meegan, C. A., & Fishman, G. J. 1996, ApJ, 459, 393
Norris, J. P., Nemiroff, R. J., Scargle, J. D., Kouveliotou, C., Fishman, G. J., Meegan, C. A., Paciesas, W. S., & Bonnell, J. T. 1994, ApJ, 424, 540
Norris, J. P., Share, G. H., Messina, D. C., Dennis, B. R., Desai, U. D., Cline, T. L., Matz, S. M., & Chupp, E. L. 1986, ApJ, 301, 213
Paciesas, W. S., Pendleton, G. N., Kouveliotou, C., Fishman, G. J., Meegan, C. A., & Wilson, R. B. 1992, in AIP Conf. Proc. 265, Gamma-Ray Bursts, ed. W. S. Paciesas & G. J. Fishman (New York: AIP), 190
Paczyński, B., & Xu, G. 1994, ApJ, 427, 708
Panaitescu, A., Wen, L., Laguna, P., & Mészáros, P. 1997, ApJ, 482, 942
Pelaez, F., et al. 1994, ApJS, 92, 651
Rees, M. J. 1966, Nature, 211, 468
Rees, M. J., & Mészáros, P. 1992, MNRAS, 258, 41
———. 1994, ApJ, 430, L93
Sari, R., Narayan, P., & Piran, T. 1996, ApJ, 473, 204
Sari, R., & Piran, T. 1995, ApJ, 455, L143
———. 1997, ApJ, 485, 270
Wen, L., Panaitescu, A., & Laguna, P. 1997, ApJ, 486, 919